

## Dynamics of Localized Magnon Modes in Antiferromagnets

SERGIO M. REZENDE

Departamento de Física, Universidade Federal de Pernambuco, Recife, 50000, PE, Brasil

and

DANIEL HONE

Department of Physics, University of California, Santa Barbara, California 93106

Recebido em 28 de Novembro de 1984

**Abstract** Some magnetic insulators have a local magnon mode with energy just below the host spin wave band. Recent high-resolution far-infrared laser and Raman light scattering experiments with  $\text{FeF}_2:\text{Mn}^{2+}$  revealed a number of very interesting effects not observed in the more usual case where the impurity mode lies far from the spin wave band. Among these are the large enhancement of the impurity response, large impurity mode relaxation and strong frequency dependence of the host AFR mode relaxation. All of these effects can be quantitatively explained with a Green's function theory for the dynamics of the local mode. In this paper we review the remarkable variety of experimental observations on this system and the theory underlying all of them.

### 1. INTRODUCTION

The properties of localized magnon modes associated with impurities in magnetic crystals have been the subject of continuing interest for nearly two decades<sup>1</sup>. The existence of these modes was initially predicted theoretically<sup>2</sup> based on the general impurity problem first studied by Lifschitz<sup>3</sup> and applied to the electron<sup>4</sup> and phonon<sup>5</sup> cases. The antiferromagnetic fluorides with substitutional magnetic impurities were the first systems on which theory and experiment could be reliably compared. On the experimental side neutron<sup>6</sup> and Raman<sup>7</sup> scattering, as well as far-Infrared spectroscopy<sup>8</sup> were used to identify the local modes and to measure their energies. Nuclear magnetic resonance was used<sup>9</sup> to study the thermodynamics of the spins near the impurity site. Theoretically the earlier work concerned mainly the models for calculating the impurity mode energies and its thermodynamics. The early models and systems studied typically involved local modes above and well separated from the continuous spin wave band and were reviewed in detail by

**This is an invited review article.**

Cowley and Buyers<sup>10</sup>. Relatively little work was done on systems in which a local mode lies in the antiferromagnetic gap, such as  $\text{CoF}_2:\text{Mn}$  and  $\text{FeF}_2:\text{Mn}$ . The former system was investigated by neutron<sup>11</sup> and light scattering<sup>12</sup>, but apparently not much attention was paid to the anomalously high intensity of the gap modes in the earlier studies.

With the development of far-infrared (FIR) lasers, high-resolution studies of impurity modes became possible and a number of antiferromagnetic systems have recently been investigated in greater detail, revealing new interesting effects. Of special interest is the  $S$ -symmetry mode of a Mn impurity in  $\text{CoF}_2$  or in  $\text{FeF}_2$ . The energy of this mode lies just below the spin wave continuum, and its absolute and relative position can be shifted significantly by the application of external magnetic fields. The energetic proximity of localized and band minimum modes implies relatively weak localization, or substantial participation of the host spins in the neighborhood of the Mn impurity in the localized excitation. Further, the degree of this coupling to the neighborhood, or the spatial extent of the local mode, is sensitive to the applied magnetic field because of the different  $g$  factors of the host and impurity spins.  $\text{FeF}_2:\text{Mn}$  has been investigated in greater detail with FIR laser spectroscopy<sup>13</sup> and light scattering<sup>14,15</sup> techniques. The experimentally observed consequences of the involvement of the host spins in the local mode include: a) large enhancement of the impurity mode intensity; b) "frequency pulling" of the host and impurity modes; c) substantial broadening of the impurity mode and d) asymmetric lineshape of the  $k=0$  host magnon. These unusual effects have attracted considerable attention and as a result a consistent picture evolved in the last few years.

In this paper we review the recent progress made in the understanding of the dynamics of the local mode in  $\text{FeF}_2:\text{Mn}$ , as well as its consequences on the host  $k=0$  magnon. Initially we present a brief introduction to the impurity associated local mode problem in ferromagnets mainly for the benefit of those unfamiliar with the field (Section 2). In Sec. 3 we summarize the experimental results for the antiferromagnetic system  $\text{FeF}_2:\text{Mn}$ . The theory underlying the new effects observed in this system is discussed in Sec. 4-7.

## 2. LOCAL MAGNON MODES IN SIMPLE FERROMAGNETS

A magnetic substitutional impurity in a magnetic crystal interacts with its neighbors with parameters different than those characterizing the interaction between host spins. This gives rise to new eigenfrequencies which may or may not lie inside the magnon band of the host crystal. If a perturbation of the impurity spin oscillates with a frequency inside the magnon band it will excite propagating magnon modes. On the other hand if the frequency lies outside the band, the response to the perturbation will be localized and it will involve the impurity spin and its close neighbors. The degree of localization of the mode depends essentially on its energetic separation from the spin wave band.

The main physics associated with a local magnon mode includes: i) its energy and eigenfunction; ii) how it affects the thermodynamics of the impurity spin and its immediate neighbors and iii) its dynamical properties, such as relaxation rate and response to external excitation (FIR, light and neutron scattering for example). Consider for simplicity a ferromagnetic crystal with exchange interaction between nearest neighbors only, and with single-ion easy axis anisotropy interaction under a static magnetic field  $H$ , along the  $z$ -direction. The spin Hamiltonian for such a system can be written as<sup>10</sup>

$$H = \sum_{\ell} g_{\ell} \mu_B H_0 S_{\ell}^z - \sum_{\ell, \delta} J_{\ell, \ell+\delta} \vec{S}_{\ell} \cdot \vec{S}_{\ell+\delta} - \sum_{\ell} D_{\ell} (S_{\ell}^z)^2 \quad (1)$$

where  $\mathbf{R}$  represents an arbitrary site in the crystal,  $\delta$  represents the  $z$  nearest neighbor sites,  $g$  is the Landé factor,  $\mu_B$  the Bohr magneton and  $J$  and  $D$  are the exchange and anisotropy interaction parameters. If the crystal is magnetically perfect, i.e. all the parameters are the same for every site, the Hamiltonian (1) has translational symmetry, and its eigenstates are the plane wave propagating magnons  $|k\rangle$ . By transforming the spin operators into boson creation and annihilation operators  $c_k^{\dagger}$  and  $c_k$  the Hamiltonian can be cast in the form

$$H = \sum_k \hbar \omega_k c_k^{\dagger} c_k + \text{magnon interaction terms} \quad (2)$$

where  $c_k^{\dagger} |0\rangle$  is a one magnon state with wavevector  $k$  and frequency  $\omega_k$  whose dispersion relation has the familiar form depicted by the solid

line in Fig. 1. For the Hamiltonian (1) the gap energy at  $k=0$  is  $\hbar\omega_0 = g\mu_B(H_0 + H_A)$  and the maximum energy at one of the zone boundary surfaces is  $\hbar\omega_{zB} = g\mu_B(H_0 + H_A + H_E)$ , where  $H_A = (2S-1)D/g\mu_B$  and  $H_E = 2S\mathcal{J}z/g\mu_B$  are the anisotropy and exchange effective fields respectively.

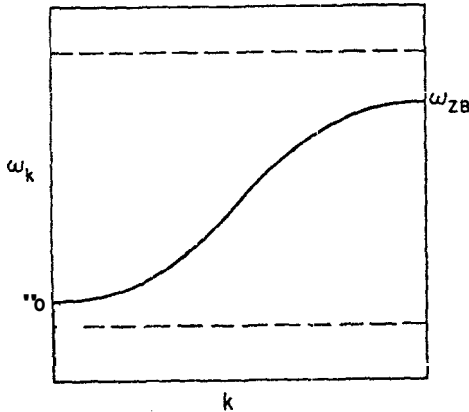


Fig.1 - Illustration of the dispersion relations for propagating (solid line) and localized (dashed lines) magnons.

Now assume that there is a single impurity ion at site,  $R = 0$  characterized by parameters  $S'$ ,  $g'$ ,  $\mathcal{J}'$  and  $D'$ . The propagating modes are slightly perturbed by the presence of the impurity and new normal modes of spin vibration appear involving the impurity and its neighbors. If the frequencies of these modes lie outside the magnon band, they are spatially localized. They are illustrated by the dashed lines in Fig.1, which reflect the fact that the local modes do not have well defined crystal momentum. If the energy of the mode for which the impurity spin vibrates more than its neighbors is well separated from the magnon band, the mode is highly localized. In this case one can assume in a first approximation that all the host spins have  $S^z = S$ , so that the exchange interaction has the simple Ising form  $\sum_{\ell} \mathcal{J} S_{\ell}^z S_{\ell+\delta}^z$ . The impurity spin thus behaves as if it were in an effective static field  $(H_0 + H'_E + H'_A)z$ , where  $H'_E = 2S\mathcal{J}'/g'\mu_B$  and  $H'_A = (2S'-1)D'/g'\mu_B$ . The impurity ( $s_0$ -symmetry) mode energy is then

$$\hbar\omega_I = g'\mu_B(H_0 + H'_E + H'_A) \quad (3)$$

This Ising approximation result does give reasonable agreement with experimentally measured energy when the local mode is far from the magnon band. Clearly the position of the impurity modes relative to the magnon band depends solely on the values of the interaction parameters

in each system. The approximation (3) fails when the mode is close to the magnon band. Moreover, it does not account for the modes with other symmetries. So a more refined treatment is necessary to describe completely the impurity mode problem. If we add and subtract to the Hamiltonian (1) with an impurity at  $\ell=0$ , the appropriate terms for a host spin at site  $\ell=0$ , it can be written as

$$H = H_0 + V \quad (4)$$

where  $H_0$  is the Hamiltonian for the pure crystal and  $V$  is a perturbation which expresses the departure of the impurity parameters from those of the host spins.  $V$  is not a small perturbation, but since it is localized around the impurity site the impurity problem can be solved to infinite order in the perturbation. In the usual procedure one uses as basis states the single spin deviation states at individual sites  $|n_\ell\rangle$ . Denoting by  $\Gamma_\lambda(\ell) = \langle n_\ell | \psi_\lambda \rangle$  the wavefunction of the eigenstate  $|\psi_\lambda\rangle$  at site  $\ell$ , Schrödinger's equation for the impurity problem can be written in the form

$$\sum_{\ell'} (H_{\ell\ell'}^0 + V_{\ell\ell'}) \Gamma_\lambda(\ell') = E_\lambda \Gamma_\lambda(\ell) \quad (5)$$

where  $H_{\ell\ell'}^0$  and  $V_{\ell\ell'}$  are the matrix elements between the states at  $\ell$  and  $\ell'$  and  $E_\lambda$  is the energy of the eigenstate  $|\psi_\lambda\rangle$ . If  $N$  denotes the number of sites in the crystal, one can define a  $N \times 1$  eigenfunction matrix  $\Gamma$  and  $N \times N$   $H^0$  and  $V$  matrices so that (5) can be written in matrix form

$$(H^0 + V) \Gamma = E \Gamma \quad (6)$$

or

$$\Gamma - G^0 V \Gamma = 0 \quad (7)$$

where

$$G^0 = (E I - H^0)^{-1} \quad (8)$$

is the Green's function matrix of the pure crystal. One can also define a Green's function for the impure crystal as  $G = (E I - H^0 - V)^{-1}$  and eq. (6) can be written as

$$G = G^0 + G^0 V G \quad (9)$$

which has the form of a Dyson equation and can be solved by methods similar to those used in other quantum physics problems. Solution of (6),

or equivalently (9), yields the energies and wavefunctions of all normal mode spin excitations in the crystal, propagating and localized. If the impurity spin interacts only with its  $z$  nearest neighbors, there are  $z+1$  impurity associated modes, with symmetries that are determined by the point group symmetry of the impurity. This was first done by Wolfram and Callaway<sup>2</sup> for a cubic symmetry ferromagnet; they had to find the energies by numerical computation. The case of a one-dimensional ferromagnet is simpler; it was first solved by White and Hogan<sup>16</sup>, who determined the energy of the p-like local mode as a function of the impurity parameters. Recently<sup>17</sup> an alternative approach to the one-dimensional problem was developed based on the transfer matrix technique. This was used for an easier determination of both the energy and wavefunction of the s-like mode, which is the one that is studied by FIR or Raman scattering measurements.

As we remarked earlier, until recently the studies of magnetic impurity modes in solids consisted mainly of the identification of the energies and symmetries of local modes in a wide variety of crystals with many different impurity ions. This led to the experimental determination of the impurity interaction parameters. The recent work on the FeF<sub>2</sub>:Mn system<sup>13-15</sup> is the first investigation of the dynamics of a local mode.

### 3. EXPERIMENTS WITH ANTIFERROMAGNETIC FeF<sub>2</sub>:Mn

In FeF<sub>2</sub>:Mn an  $s_0$ -symmetry local magnon exists just below the host spin wave band. Because of the proximity of the impurity mode to the  $k=0$  magnon energy, the local mode wavefunction is spatially extended so that there is a substantial participation of the host Fe<sup>2+</sup> neighbor spins in the impurity mode excitation. Due to the two spin sublattices of the system, an impurity spin energy can shift either upward or downward with the applied field  $H$ , depending on the sublattice on which the impurity site is located. Because of the spatial extent of the  $S_0$ -modes, the experiments reveal unusual effects, such as: a) large enhancement of the impurity mode intensity; b) "frequency pulling" of the host and impurity modes; c) substantial broadening of the impurity mode and d) asymmetric lineshape of the  $k=0$  host magnon. Effects a, c and d can be seen in the FIR transmission spectrum<sup>13</sup> of a

$\text{FeF}_2$  sample with Mn impurity concentration  $x=0.0014$  at.% obtained with a  $\text{H}_2\text{O}$  molecular laser, shown in Fig. 2. The spectrum is obtained by

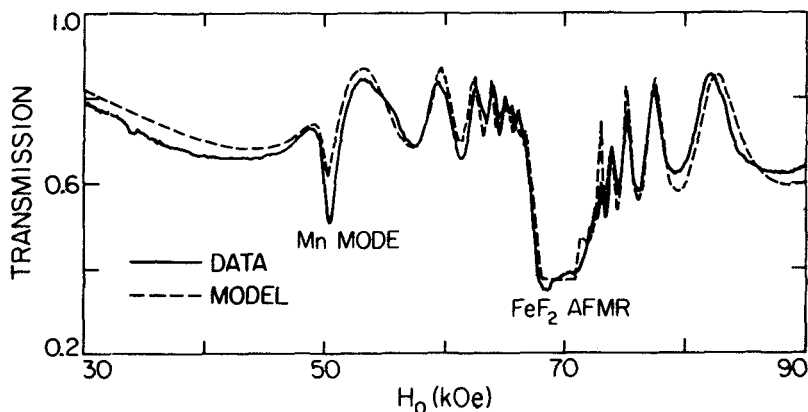


Fig.2 - Transmission data of a  $\text{FeF}_2:\text{Mn}$  disk with thickness  $786 \mu\text{m}$  obtained with a  $\text{H}_2\text{O}$  laser at  $1.36 \text{ THz}$  by sweeping the magnetic field. The Mn Impurity concentration is  $0.0014$  at.%. The dashed line is the theoretical prediction of the polariton model. After ref. 13.

sweeping the external magnetic field  $H$ , parallel to the  $c$  axis of the crystal, so that the down-going impurity and host modes are brought into resonance with the laser frequency  $\nu=1.362 \text{ THz}$  as illustrated in Fig. 3. Full details of the experiments are given by Sanders *et al.*<sup>13</sup>. Because of the coupling between electromagnetic and spin waves, the FIR transmission spectrum of the host mode exhibits a broad lineshape with a flat section characteristic of the forbidden gap of the polariton dispersion curve. As a consequence the data must be obtained by fitting the spectrum to the theoretical prediction of a polariton model, which can be done quite accurately, as shown in Fig. 2.

The effects described above have also been observed in inelastic light scattering experiments<sup>14,15</sup>. In these measurements one probes magnons with wavevectors  $k \sim 10^5 \text{ cm}^{-1}$  which is far from the polariton region ( $k \sim 10^3 \text{ cm}^{-1}$ ), so that the scattering lineshapes reflect the true magnon behavior. Fig. 4 shows two light scattering spectra: (a) obtained with a double monochromator in standard Raman scattering experiment for a sample with  $x = 0.28\%$  and  $0.75\%$  at  $H_c = 0$ ; (b) spectrum of a  $x = 0.5$  at.% sample in  $H_c = 0$  obtained by analyzing the scattered light with a

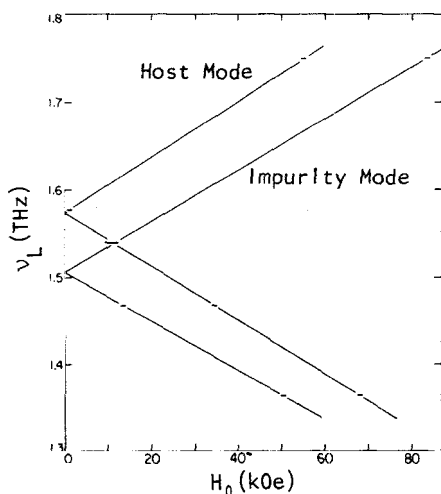


Fig.3 - Field dependence of the up- and down-going host and impurity modes in  $\text{FeF}_2:\text{Mn}$  with  $x \approx 0.01$  at.%. The horizontal dashes indicate typical FIR laser frequencies.

Fabry-Perot Interferometer. In contrast to the spectrum in 4a obtained earlier<sup>14</sup>, the more recent result<sup>15</sup> shown in Fig. 4b shows that the impurity and host modes have clearly distinct lineshapes and widths. The light scattering experiments have been used to measure the relative intensities of the local and host modes and the linewidths for impurity concentrations  $x \geq 0.3$  at.%. However, due to its higher resolution the FIR transmission technique has provided more detailed measurements of the relaxation of both modes. In each of the following sections we present a brief account of the main experimental results obtained with the two techniques and give their theoretical interpretation.

#### 4. ENHANCEMENT OF THE IMPURITY MODE RESPONSE

The most striking feature of the spectra in Figs. 2 and 4 is the surprisingly large integrated intensity of the impurity mode response, typically comparable to that of the host mode even at impurity concentrations below 1 at.%. In the light scattering spectrum the enhancement of the impurity mode is even more surprising than in the FIR data in view of the weak photon coupling to the  $\text{Mn}^{2+}$  S-symmetry ground state. The high intensity here arises indirectly through the oscillating transverse component of the exchange fields of the  $\text{Fe}^{2+}$  neighbor spins which couple strongly to the radiation fields. This problem was initially treated within a simple sublattice model which attributes an equal magnetization to every host spin (regardless of its position



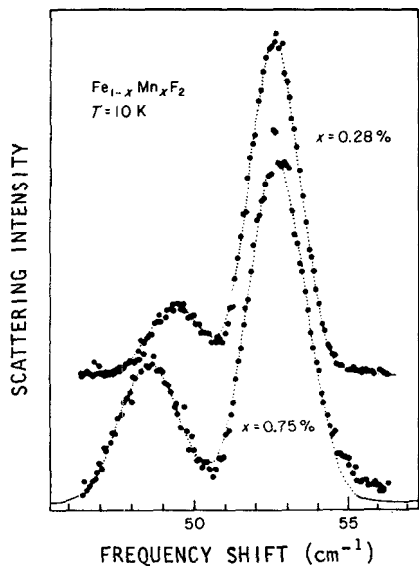


(Fig.4a)

Fig.4 - Spectra of inelastic scattering of light by the host and local magnon modes in  $\text{FeF}_2:\text{Mn}$ . a) Obtained by Raman scattering techniques with  $x = 0.28$  and  $0.75\%$ . b) Obtained with a Fabry - Perot interferometer with  $x = 0.5\%$ .

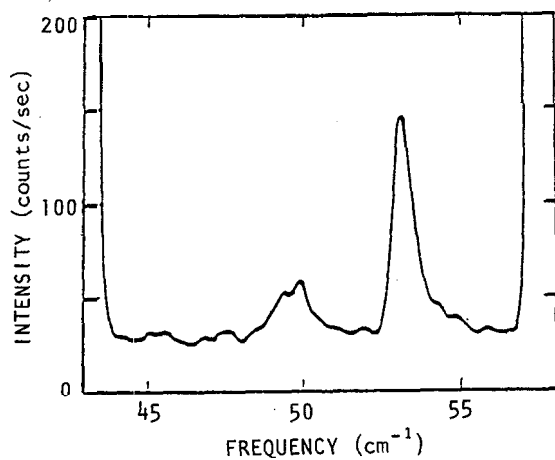


(Fig. 4b)

relative to an impurity), and similarly for the impurity spins, and solving the coupled equations of motion of these magnetizations. This approach explains the enhancement of the infrared and Raman impurity intensities only qualitatively. The correct calculation must take into account the spatially extended character of the local mode. This has been done using zero-temperature Green's functions in the limit of a single impurity in the crystal<sup>18</sup>. The theory is based on a simple model Hamiltonian for FeF<sub>2</sub>:Mn which includes isotropic exchange, single-ion uniaxial anisotropy along the c axis of the lattice (chosen here as the z direction) and the Zeeman interaction with a magnetic field H, applied along the c-axis

$$\begin{aligned}
 H = \mu_B H_0 \sum_{\ell} g_{\ell} S_{\ell}^z + 2J_2 \sum_{\ell, \delta} \vec{S}_{\ell} \cdot \vec{S}_{\ell+\delta} - D \sum_{\ell} (S_{\ell}^z)^2 \\
 + 2J_2' \vec{S}_0 \cdot \sum_{\delta_2} \vec{S}_{\delta_2} + 2J_1' \vec{S}_0 \cdot \sum_{\delta_1} \vec{S}_{\delta_1} - D' (S_0^z)^2
 \end{aligned}
 \tag{10}$$

where sites are labeled by subscripts on the spin operators and a single impurity is located at the origin ( $\ell=0$ ). We have retained only the dominant exchange terms, between next-nearest neighbors on opposite sublattices of the body-centered tetragonal arrangement of magnetic atoms, for the pure FeF<sub>2</sub> host, or between Fe spins. The impurity spin is taken to couple with its eight next-nearest neighbors at positions  $\delta_2$ , and its two nearest neighbors at positions  $\delta_1$ . The magnetic response of the system to a uniform electromagnetic field (frequency  $\omega$ ) is given by the relevant frequency dependent uniform susceptibility<sup>19</sup>

$$\chi^{++}(\omega, q=0) = \frac{\pi}{\hbar V} \sum_{\ell, \ell'} m_{\ell} m_{\ell'} \langle\langle S_{\ell}^+; S_{\ell'}^- \rangle\rangle_{\omega}
 \tag{11}$$

where  $m_{\ell}$  expresses the strength of the coupling between the radiation fields and the spin  $\vec{S}_{\ell}$ ,  $V$  is the volume of the crystal and  $\langle\langle S_{\ell}^+; S_{\ell'}^- \rangle\rangle_{\omega}$  is the time Fourier transform of the retarded Zubarev Green's function<sup>20</sup> for the spin operators. In order to find  $\chi^{++}$  one must solve the equations of motion for the Green's functions of the impure spin system. This is easily done if the spin operators are expressed in terms of the boson operators  $c_{\alpha}$  and  $c_{\beta}$  which diagonalize the quadratic part of the Hamiltonian (10). These are introduced by

These determine the eigenfrequencies and the normal mode amplitudes associated with the impurity  $A$  and its interacting neighbors  $A_{\delta_1}$  and  $A_{\delta_2}$ , subject to the orthonormality condition (13). Note that there are only 3 amplitudes here because only a totally symmetric  $s_0$ -mode is being considered. With the knowledge of these amplitudes and the crystal Green's functions one can find the wave function at any site in the crystal. From eqs. (7), (14) and (15) one has<sup>18, 22</sup>

$$\Gamma = G^0 A$$

or

$$\Gamma_{\lambda}^{\lambda}(\pm\omega) = G_{\lambda 0}^0(\omega) A_0^{\lambda} + \sum_{\delta_1} G_{\lambda \delta_1}^0(\omega) A_{\delta_1}^{\lambda} + \sum_{\delta_2} G_{\lambda \delta_2}^0(\omega) A_{\delta_2}^{\lambda} \quad (16)$$

There are four types of pure crystal Green's functions that can be expressed in terms of their Fourier-transforms

$$G_{k\lambda}^0(\sigma)(\omega) = \frac{1}{N} \sum_k e^{i\vec{k} \cdot (\vec{r}_m - \vec{r}_\lambda)} G_k^{(\sigma)}(\omega) \quad (17)$$

where  $\sigma = 1$  for  $m$  and  $R$  in sublattice  $i$ ,  $\sigma = 2$  for  $m = i$ ,  $R = j$ ,  $\sigma = 3$  for  $m = j$ ,  $R = i$ , and  $\sigma = 4$  for  $m = j$ ,  $R = j'$ . These Green's functions can be easily obtained<sup>18</sup>

$$\begin{aligned} G_k^{(1)}(\omega) &= \frac{\omega' + \omega_E + \omega_A}{\omega'^2 - \omega_k^2} \\ G_k^{(2)}(\omega) &= -G_k^{(3)}(\omega) = -\frac{\gamma_k \omega_E}{\omega'^2 - \omega_k^2} \\ G_k^{(4)}(\omega) &= \frac{\omega' - (\omega_E + \omega_A)}{\omega'^2 - \omega_k^2} \end{aligned} \quad (18)$$

where  $\omega' = \omega + \omega_H$ ,  $\hbar\omega_H = g\mu_B H_0$ ,  $\hbar\omega_E = 2S_z J$ ,  $\hbar\omega_A = (2S-1)D$ ,  $\gamma_k$  is the usual structure factor which appears in the spin-wave frequencies.

$$\begin{aligned} \omega_{\alpha} &= \omega_k \pm \omega_H \\ \beta & \\ \omega_k &= [(\omega_E + \omega_A)^2 - \gamma_k^2 \omega_E^2]^{1/2} \end{aligned} \quad (19)$$

The cluster formed by the Impurity, its two nearest, and its eight next-nearest neighbors in the rutile structure belongs to the symmetry group  $D_{4h}$  whose irreducible representations are  $3A_{1g} + 2A_{2u} + B_{1u} + B_{2g} + E_g + F_u$ . The three  $A_{1g}$  modes have s-like wave functions which are even and non-zero at the impurity site. For the  $s$  modes we make  $A_{\delta_1} \equiv A_1$  and  $A_{\delta_2} \equiv A_2$ . Eq. (15) can be solved as in ref. 18, and the wavefunctions are easily obtained with eq. (16). The total Hamiltonian (10) is diagonal (in the noninteracting magnon approximation) in the normal mode operators  $c_\lambda$  and  $c_\lambda^\dagger$ , so that the equations of motions for the Green's functions of the various pairs of operators  $c_\lambda$  and  $c_\lambda^\dagger$  can be solved exactly, leading to

$$\begin{aligned} \langle\langle c_\lambda; c_{\lambda'}^\dagger \rangle\rangle_\omega &= \frac{1}{2\pi} \frac{\delta_{\lambda\lambda'}}{\omega - \omega_\lambda} \\ \langle\langle c_\lambda^\dagger; c_{\lambda'} \rangle\rangle_\omega &= \frac{-1}{2\pi} \frac{\delta_{\lambda\lambda'}}{\omega + \omega_\lambda} \\ \langle\langle c_\lambda; c_{\lambda'} \rangle\rangle_\omega &= \langle\langle c_\lambda^\dagger; c_{\lambda'}^\dagger \rangle\rangle_\omega = 0 \end{aligned} \quad (20)$$

With the transformations inverse to (12) and (20), the susceptibility (11) at frequencies  $\omega$  near the s-local mode frequency  $\omega_s$  becomes<sup>18</sup>

$$\begin{aligned} \chi(\omega = \omega_s) &= \frac{m^2 S}{\hbar V} \frac{1}{\omega - \omega_s} \left\{ \sum (-1)^{\ell\ell'} \Gamma_\ell^{s*} \Gamma_{\ell'}^s, \right. \\ &\quad \left. - \left[ \left( \frac{m'}{m} \sqrt{\frac{S'}{S}} - 1 \right) \Gamma_0 \left( \sum \Gamma_i^{s*} - \sum \Gamma_j^s \right) - \text{c.c.} \right] \right\} \end{aligned} \quad (21)$$

Eq. (21) shows that the response of the local mode depends on how far the wavefunction spreads over the impurity neighbors. The summations in eq. (21) can actually be evaluated analytically using eq. (16). They lead to the  $q=0$  components of the Fourier transform of the pure crystal Green's functions (18), which measure the response of the host magnons to a uniform ( $q=0$ ) excitation. Assuming that there are  $Nx$  non-interacting impurities in each sublattice the total susceptibility near an  $s$ -mode frequency becomes

$$\chi(\omega = \omega_s) = \frac{Nm^2 S}{\hbar V} \left[ \frac{2\Gamma_0^s \mu B(\omega)}{[(\omega_s + \omega_H)^2 - \omega_0^2]} - \frac{B(\omega)^2}{[(\omega_s + \omega_H)^2 - \omega_0^2]^2} \right] \frac{1}{\omega - \omega_s} \quad (22)$$

where

$$c_{\alpha} = \sum_i (2S_i)^{-1/2} \Gamma_i^{\alpha} S_i^{+} + \sum_j (2S_j)^{-1/2} \Gamma_j^{\alpha} S_j^{+} \quad (12)$$

$$c_{\beta}^{+} = \sum_i (2S_i)^{-1/2} \Gamma_i^{\beta} S_i^{-} + \sum_j (2S_j)^{-1/2} \Gamma_j^{\beta} S_j^{-}$$

where  $i$  and  $j$  denote the sites of the up and down spin sublattices respectively and  $\alpha$  and  $\beta$  denote the normal modes (propagating and localized) which shift up or down with the magnetic field respectively. The wavefunctions obey the orthonormality relations

$$\sum_i \Gamma_i^{\lambda} \Gamma_i^{\lambda'^{*}} - \sum_j \Gamma_j^{\lambda} \Gamma_j^{\lambda'^{*}} = \pm \delta_{\lambda\lambda'} \quad (13)$$

where the positive sign holds for the  $\alpha$  mode and the negative for the  $\beta$  one. Clearly the treatment of antiferromagnets<sup>21-22</sup> is more cumbersome than for ferromagnets because of the two-sublattice nature of the problem. However, the equations of motion can be cast in the same form as those in Section 2 by defining suitable matrices made up of submatrices characteristic of the two sublattices. The eigenvalue equation then has the same form as (7). Its solution yields the normal mode energies and wave functions, subject to the condition of eq. (12). Due to the finite range of the perturbation caused by the impurity the solution of eq. (7) reduces to solving a set of  $11 \times 11$  secular equations (for the assumed form<sup>10</sup> of the Hamiltonian). The calculation of the corresponding determinant can be simplified by block diagonalization of the matrix  $\mathbf{G}^0 \mathbf{V}$ . This can be accomplished via a unitary transformation from a basis of individual sites to linear combinations that transform according to the irreducible representations of the symmetry group of the cluster formed by the impurity and its interacting neighbors. The  $11 \times 11$  unitary transformation for this case has been given by Shiles and Hone<sup>23</sup>. Instead of the site wave functions a more convenient set of normal mode amplitudes<sup>18</sup> can be used to solve (7). They are represented by the  $11 \times 11$  column matrix  $\mathbf{A}$  obtained from  $\mathbf{\Gamma}$  by the transformation,

$$\mathbf{A} = \mathbf{V} \mathbf{\Gamma} \quad (14)$$

Equations (7) and (14) lead to a new set of secular equations,

$$(\mathbf{I} - \mathbf{V} \mathbf{G}^0) \mathbf{A} = \mathbf{0} \quad (15)$$

$$\mu = \frac{m'}{m} \left[ \frac{S'}{S} \right]^{1/2} - 1$$

$$B(\omega) = \omega_E (A_0^S + 2A_1^S) (\omega^+ - 1) - 8\omega_E A_2^S (\omega^- + 1)$$

where  $\omega^\pm = (\omega' \pm \omega_A \pm \omega_E)/\omega_E$ . Eq. (22) shows that the intensity of the local mode increases rapidly as its frequency approaches the  $q=0$  magnon frequency  $\omega_0 - \omega_H$ . This results from the fact that the wavefunction of the local mode close to the  $q=0$  magnon spreads over many impurity neighbors, leading to a large enhancement of the impurity response, as observed in the experiments on  $\text{FeF}_2:\text{Mn}$ . An enhancement, not as large as in  $\text{FeF}_2:\text{Mn}$  has also been observed<sup>24,25</sup> in  $\text{CoF}_2:\text{Mn}$  in which the  $q=0$  magnon is at  $-35 \text{ cm}^{-1}$  and the impurity mode is at  $-28 \text{ cm}^{-1}$  at  $H_0=0$ . In a neutron scattering experiment with momentum transfer equal to the zone-boundary wavevector  $q_{z\bar{b}}$ , one should observe a similar enhancement for local modes above the magnon band and near the frequency  $\omega_{z\bar{b}}$ , such as in  $\text{FeF}_2:\text{Co}$ <sup>26</sup>. The large enhancement observed in  $\text{FeF}_2:\text{Mn}$  has been explained quantitatively with the theory above. The impurity s-mode energy, wavefunction and dynamic response for this system have been calculated in detail in ref. 18. Comparison with the energy and relative intensity measurements have allowed the determination of the impurity-host exchange interaction parameters  $J_1' = 0.2 \text{ cm}^{-1}$ ,  $J_2' \approx 1.79 \text{ cm}^{-1}$ , both antiferromagnetic.

## 5. FREQUENCY PULLING

Another evidence of the strong coupling between the local mode and the  $q=0$  magnon in  $\text{FeF}_2:\text{Mn}$  is the pulling of their frequencies relative to the values in the single impurity limit. Relative frequency shifts are of order a percent for 0.1 at.% impurity. Fig. 5 shows the measured frequencies at  $H_0=0$  versus impurity concentration<sup>13</sup>. The light scattering data are obtained directly from the spectra. The FIR values are obtained by extrapolating the data to zero field. The curves shown are the frequency pulling predictions of the magnetization coupled mode model for various choices of the exchange interaction parameter  $\lambda_1'$  between the impurity and the two nearest neighbors. Though the coupled magnetization model gives a good description of the frequency pulling as a function of  $x$ , it requires parameters which correspond to interac-

tion constants  $J_1^I \approx 2.0 \text{ cm}^{-1}$  and  $J_2^I = 2.04 \text{ cm}^{-1}$ <sup>13</sup>. These are very different from the values which explain a wide range of other phenomena (including the local mode response just discussed). In particular,  $J_1^I$  is far too big. Actually it is not surprising that the coupled magnetization model does not yield the correct parameters because in the limit  $x=0$  it gives the Ising model frequencies, a result which is known to

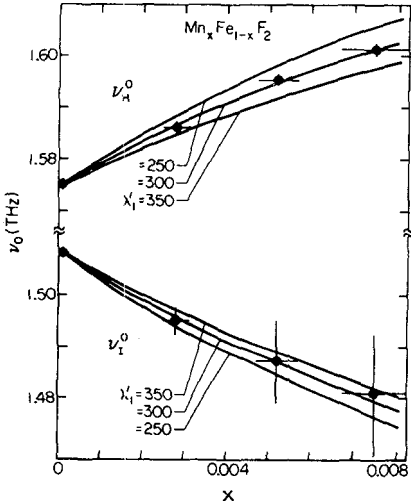


Fig.5 - Zero-field resonance positions of both host and impurity modes obtained by extrapolating to  $H_0=0$  the values measured at several FIR laser frequencies (ref. 13).

fail if the impurity mode is not sufficiently localized. The correct theory for the energies at finite impurity concentrations has yet to be developed. Of course, this problem cannot be treated within the single spin formalism presented earlier.

## 6. LOCAL MODE LINEWIDTH

Fig. 6 shows the impurity mode line width data obtained from the low temperature FIR transmission spectra of several samples with different impurity concentrations and different thicknesses. Three main mechanisms have been identified<sup>13</sup> for the broadening of the local mode in  $\text{FeF}_2:\text{Mn}$  at low temperatures, namely: i) Radiation damping, ii) Single impurity processes and iii) Impurity-impurity interaction. The radiation damping mechanism<sup>27</sup> is greatly enhanced by the participation of the  $\text{Fe}^{2+}$  spins in the local mode and is the source of the linear dependence of the linewidth on the sample thickness, as shown in detail in

ref. 13. Extrapolation of the data of Fig. 6 to zero thickness gives the intrinsic linewidth of the local mode. Impurity banding effects<sup>2,8</sup> are responsible for the concentration dependence of the linewidth but they cannot account for the large residual value of about 1kOe as  $x \rightarrow 0$ . The latter is due to single impurity damping processes, which have recently been studied theoretically<sup>2,9</sup>. For the up-going local mode, anisotropy and dipolar interactions which break the spin-rotational symmetry about the field axis provide<sup>30</sup> a mechanism for the decay of the local modes into band magnons in the frequency range 1.54-1.93 THz. However, since the down-going mode is energetically the lowest-lying magnetic excitation in the system, other excitations must be involved in the relaxation process.

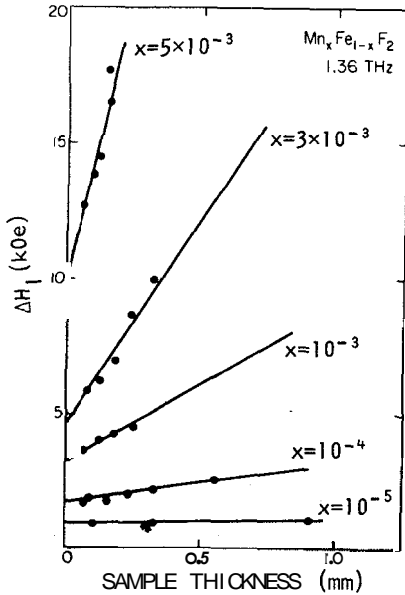


Fig.6 - Impurity mode linewidth measured by FIR laser spectroscopy for several Mn concentrations in FeF<sub>2</sub> vs. sample thickness. The straight lines are best fits to the data; their slopes determine the radiation damping contribution to  $\Delta H_1$ .<sup>13</sup>

At least two arguments suggest that phonons play a dominant role in the damping: Acoustic phonons are the only collective excitations in FeF<sub>2</sub> with energies below the Mn impurity mode, and the magnetic moments ("spins") of the Fe<sup>2+</sup> ions that participate in the local-mode excitation couple strongly to lattice vibrations. In pure FeF<sub>2</sub> phonons do not contribute to the relaxation of magnons because their



dispersion relations are very different; thus energy and momentum cannot be conserved simultaneously. But in Mn-doped  $\text{FeF}_2$  there is no translational symmetry around the impurities, and the requirement of momentum conservation is relaxed. Fig. 7 illustrates possible decay processes. The coupling between spins and lattice vibrations arises from several sources, but in  $\text{FeF}_2$  it has been shown<sup>31</sup> that the dominant mechanism is phonon modulation of the crystal field, which can be calculated from first principles. Using the spin-lattice interaction in  $\text{FeF}_2$  and the results of the Green's function calculation of the impurity mode properties in  $\text{FeF}_2:\text{Mn}$ , it has been shown<sup>29</sup> that two phonon assisted processes can effectively relax the local mode: one is the direct decay into a degenerate acoustic phonon and the other is the decay into a magnon-phonon pair.

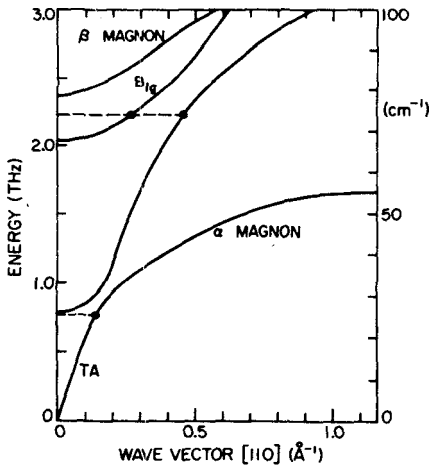


Fig.7 - Illustration of possible processes for the decay of a local magnon into phonons. A mode in the down-going branch can decay into an acoustic phonon. An up-going mode can decay into an acoustic and an optical phonon (ref.29).

The interaction Hamiltonian for the decay of the local mode into an acoustic phonon can be written as<sup>29</sup>

$$H_{\text{int}} = -i(\hbar S^3/MN)^{1/2} b \sum [q/\omega_q^{1/2}] F(q) a_q^\dagger c_s + \text{h.c.} \quad (23)$$

where  $a_q^\dagger$  is the creation operator of the phonon with frequency  $\omega_q$ , the form factor  $F(q)$  is essentially the Fourier transform of the magnon wave function at the phonon wave vector

$$F(q) \equiv \sum_{\ell \neq 0} e^{-i\vec{q} \cdot \vec{r}_\ell} \Gamma_\ell^* \quad (24)$$

and  $b$  is a magnetoelastic coupling coefficient

$$b = \frac{\lambda^2 (2S - 1) P \delta}{\sqrt{2} \Delta_{xy} \Delta_{xz} S} \quad (25)$$

where  $\lambda$  is the spin-orbit coupling constant of the  $\text{Fe}^{2+}$  ions,  $P$  is a Coulomb matrix element and  $\Delta_{xy}$  and  $\Delta_{xz}$  are crystal-field energy splittings defined in ref. 31. The form factor  $F(q)$  in (24) measures the extent of spatial matching of the magnetic and phonon excitations, excluding the impurity spin at  $R=O$  because the  $\text{Mn}^{2+}$  ion does not couple to the crystal field. With the wavefunctions calculated by (16) the form factor has been given explicitly for the  $\epsilon_0$  local mode<sup>29</sup>.

In general, the local magnon can decay into any phonon energetically degenerate with it (unless other symmetries prevent magnon-phonon coupling). In  $\text{FeF}_2$  the transverse-acoustic phonon bands extend as high as 3 THz, and above 2.04 THz the magnon also becomes degenerate with phonons in the  $B_{1g}$  optical band, but the contribution from the optical phonon to the linewidth has been shown to be negligible. At temperatures low compared with the local-magnon energy, where the number of thermally excited phonons degenerate with that magnon is negligible, the standard golden-rule calculation gives for the decay rate of the local mode into acoustic phonons a contribution

$$\Delta H_{TA} = \frac{S^3 b^2 q_0^4 |F(q_0)|^2}{\pi \gamma \hbar \rho \omega_s (c_0 - 3c_1 q_0^2)} \quad (26)$$

where  $\rho$  is the mass density,  $F(q_0)$  is the local mode form factor,  $q_0$  is the wave number of the phonons degenerate with the local magnon  $\omega(q_0) = \omega_s$ ,  $(c_0 - 3c_1 q_0^2) = d\omega/dq$  characterize the acoustic phonon density of states in our approximation of the dispersion relation, and  $\gamma$  is the gyromagnetic ratio ( $\gamma \hbar = g \mu_B$ ).

When the up-going mode has frequency above 1.54 THz ( $H_0 > 11$  kOe), it can decay into an acoustic phonon-down-going propagating magnon pair. The contribution of this process to the linewidth is<sup>29</sup>

$$\Delta H (m+p\hbar) \approx \frac{S^2 b^2 \Omega}{4\pi^4 \gamma \hbar \rho} \int d^3k q_0^3(k) [\mathcal{C}(\vec{k}, \vec{q}_0)]^2 / c_0^2 \quad (27)$$

where  $q_0(k)$  is the phonon wave vector demanded by energy conservation, C is another suitably defined form factor and R the unit cell volume. The linewidths given by (26) and (27) were evaluated numerically for FeF<sub>2</sub>:Mn. Their dependences on the local mode energy are shown in Fig. 8 by curves A and B. The obvious  $\omega^3$  dependence (from  $q_0^4/\omega_s$ ) in eq. (26) is dominated by the rapid falloff of the form factor  $F(q_0)$  above  $q_0$  of the order of the inverse of the local magnon size, so curve A decreases with  $\omega$ . Note that the ranges below and above 1.507 THz correspond to the down-going and up-going local modes respectively. As pointed out in ref. 29, near 1.7 THz there is a strong admixture of magnons and phonons and the actual normal modes are magnetoelastic excitations. But far from this region the bare phonon is a good approximation to the excitation into which the local mode decays. The data point at 1.36 THz in Fig. 8 is the residual impurity mode linewidth obtained from Fig. 6 and it is clearly accounted for by the calculation described above. The bars at 0.85 and 2.5 THz represent data taken at the High Magnetic Field laboratory of Osaka University<sup>32</sup> and both are also in good quantitative agreement with the theory.

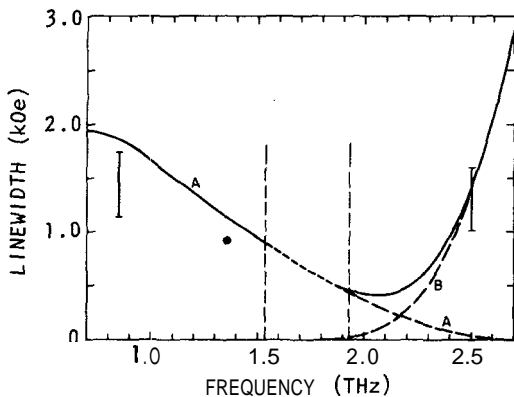


Fig.8 - Residual local-mode linewidth from phonon-associated relaxation processes. Theoretical curves are labelled A (decay into a phonon) and B (phonon-magnon pair)<sup>29</sup>. In the region between 1.54 and 1.93 THz  $S_z$ -nonconserving magnetic decay also contributes to the linewidth<sup>30</sup>. Data are represented by the dot and the vertical bars<sup>13,32</sup>.

Within the frequency range 1.54-1.93 THz marked by vertical dashed lines in Fig. 8, the up-going local mode is degenerate with the down-going magnon band. Thus in this region the local mode can decay into the magnetoelastic excitations not only via the coupling to phonons as already discussed (and represented by the dashed extensions of curve

A in the figure), but also in principle via explicitly magnetic interactions to the magnon component of the final states. This does *not* occur through the dominant magnetic Hamiltonian (10), because that operator is invariant to spin rotations about the  $z$ -axis, whereas the decay process here requires a single spin flip (the initial and final excitations being on the up-going and down-going branches, respectively). But there are small magnetic interaction terms, otherwise negligible, which do break this spin rotational symmetry. The most obvious of these is the magnetic dipole-dipole Hamiltonian

$$H_d = (\hbar^2/2) \gamma^2 \sum [\vec{S}_i \cdot \vec{S}_j - 3(\vec{S}_i \cdot \hat{r}_{ij})(\vec{S}_j \cdot \hat{r}_{ij})] r_{ij}^{-3} \quad (28)$$

In addition, there is an orthorhombic magnetocrystalline anisotropy term associated with the electrostatic fields of the ions surrounding a  $\text{Fe}^{2+}$  site. Although the dominant departure of the environment from cubic symmetry is the tetragonal distortion measured by the uniaxial term  $D(S_z^2)^2$  in eq. (10), there is also a smaller symmetry in the  $x$ - $y$  plane, leading to the term

$$H_{oa} = -(E/2S) \sum \eta_i [(S_i^x)^2 - (S_i^y)^2] \quad (29)$$

where  $\eta_i$  is +1 for  $i$  on the up sublattice and -1 for  $i$  on the down sublattice, because the  $F^-$  cage is rotated by  $\pi/2$  about the  $z$  axis in going from a magnetic site on one sublattice to one on the other. Thus, there is a local, but not global, orthorhombic anisotropy.

Independent calculations of this  $S_2$ -nonconserving magnetic decay mechanism<sup>30</sup> and the phonon-associated mechanism discussed above demonstrate that the two contributions to the linewidths are expected to be comparable. Since the final states involved are the same, we should properly take into account the quantum interference between the amplitudes for the two processes in calculating the total probability for decay; the corrections from the interference terms may well be large. However, to carry out the amplitude calculation for the symmetry-breaking anisotropy interaction to find both magnitude and phase, we need the final-state wave function. The impurity offers primarily a magnetic contrast to the host atoms, and as opposed to the phonon final states we have considered above, which are well represented as plane

waves, the continuum magnons are distorted from plane waves precisely in the neighborhood of the impurity, where their overlap with the initial local mode state is substantial. This difficulty is avoided in the approach of ref. 30 where the local impurity susceptibility is calculated directly; its imaginary part measures the local mode linewidth contribution from the dipolar and orthorhombic anisotropy interaction included. As is common to Green's function calculations this one has the advantage of not demanding explicit knowledge of the form of the wave functions, but the price paid is that it also does not yield the essential information about the phase of the transition amplitudes. We do not know whether constructive interference, a slightly larger orthorhombic anisotropy constant  $E$  than estimated in ref. 30 or a combination of these may explain the relatively large observed linewidth of 3 kOe at 1.75 THz, as compared with a combined theoretical value of about 1 kOe from the two mechanisms treated independently. But we do note that a factor of 2 in the anisotropy constant or completely constructive interference would each essentially remove the discrepancy, and neither seems unreasonable. It is also conceivable that there may be other symmetry breaking interactions, including anisotropic exchange or Dzialoshinski-Moriya interactions, which make substantial contributions to the linewidth here. However, none of these has been demonstrated to exist by independent experiment.

At sufficiently low impurity concentrations it is reasonable and useful to view the concentration dependence of the local mode linewidth as arising from the spatial overlap of the wave functions of local magnons centered on different impurities. To second order in the concentration one effectively sums the results of the dynamical interactions of impurity pairs over a random spatial distribution of impurities. The four Green's functions labeled by the sites of the single pair of the two impurity problem are coupled by the equations of motion. We are interested in the behavior of the system near the local mode frequency  $\omega = \omega_s$ ; the parts of the Green's functions singular at  $\omega = \omega_s$  can be reproduced by an effective interaction<sup>28</sup>

$$H_{\text{eff}} = \omega_s \sum_i c_i^\dagger c_i - \sum_{i,j} V_{ij} c_i^\dagger c_j \quad (30)$$

where  $c_i$  destroys a local mode associated with the impurity site  $i$ , and we have written the Hamiltonian for the full system as a sum of pairwise interactions. Clearly at higher concentrations one would have to modify the effective medium which moderates the interactions between local modes. We have essentially calculated the uniform magnetic susceptibility appropriate to this Hamiltonian averaged over impurity distributions. More accurately, we have calculated the frequency moments of the imaginary part of the susceptibility, which is directly related to the absorption lineshape, again to second order in concentration.

The predictions of the theory for the linewidth are compared with experiment at  $H_0 \approx 50$  kOe with a laser frequency of 1.36 THz in Fig. 9. With the inclusion of an independent single impurity phonon-related width of 1 kOe, as calculated earlier, we find excellent quantitative agreement. It is true that the concentration dependence is relatively weak, but we emphasize that there are no adjustable parameters. For completeness in Fig. 9 we compare the results with the predictions for a system with perturbation strength twice as large, which could not be

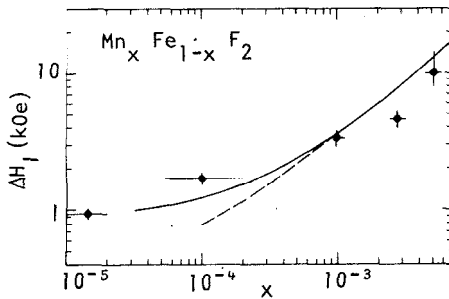


Fig.9 - Concentration dependence of the impurity banding contribution to the local mode linewidth<sup>28</sup>. Data are obtained at 1.36 THz<sup>13</sup>.

reconciled with this experiment. In Fig. 10 we compare the  $H_0=0$  light scattering linewidth data with the results of phonon decay and impurity banding calculation the latter scaled inversely proportional to the local mode  $k=0$  magnon energy splitting. Again the agreement is quite good. More directly and unambiguously affected by impurity parameters are the positions of satellite resonance lines associated with Mn impurity pairs in various spatial positions. We have successfully identified<sup>33</sup> six such experimental lines with the predictions of theory. The agreement is

quantitative with Impurity parameters  $J' \approx 0.5 \text{ cm}^{-1}$ , and  $J'' \approx 1.8 \text{ cm}^{-1}$ , in agreement with the values found necessary to explain the enhancement and linewidth data above.

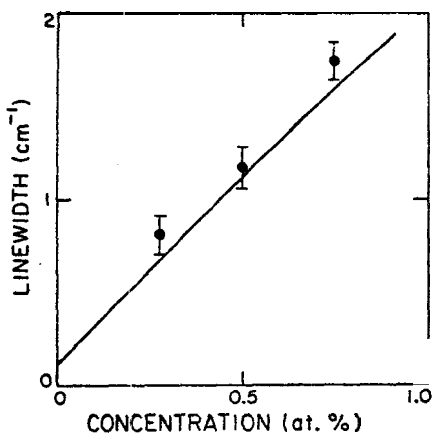


Fig.10 - Comparison between the local mode linewidth data<sup>15</sup> in  $\text{FeF}_2:\text{Mn}^{2+}$  and the prediction of theory as a function of the impurity concentration. The solid line represents the sum of phonon assisted<sup>29</sup> and impurity banding<sup>28</sup> processes.

## 7. HOST MODE LINESHAPE

As we remarked earlier, the lineshape of the FIR transmission spectrum of the host mode in  $\text{FeF}_2:\text{Mn}$  is dominated by the polariton nature of the propagating magnetic mode in the sample. Nevertheless, by letting  $\omega \rightarrow \omega + i\gamma\Delta H/2$  in the coupled magnetization equations of motion, the linewidth of the host mode can be obtained from the lineshape by carefully fitting the experimental spectrum to the calculated transmission. The most significant features of the data are: i) the relaxation rate of the host mode is lower than that for the impurity mode; ii) the linewidths increase rapidly with the impurity concentration and iii) the relaxation rate increases with increasing frequency. All of these features are confirmed by the light scattering measurements<sup>15</sup>.

The first attempt to explain the host mode linewidth based on impurity exchange and anisotropy scattering led to values above the polariton gap which were more than two orders of magnitude smaller than the data. The reason for this failure is that the perturbation potential associated with the Mn impurity is so strong that the spatially extended local mode appears; hence, the usual perturbation theory (Fermi Golden Rule) is not directly applicable. It has been shown that inclusion of

multiple scattering effects (from a single impurity) corrects this problem and accounts for the observed linewidths<sup>34</sup>.

The broadening mechanism for the host mode is a two magnon scattering, in which a magnon of wavevector  $k$  decays via impurity scattering into degenerate magnons with  $\vec{k}' \neq \vec{k}$ . In the usual situation where the impurity mode is far from the spin wave band, the linewidth is calculated by the standard Golden Rule expression<sup>35</sup>

$$\Delta H(\omega) = \frac{\Omega}{\gamma \hbar^2 (2\pi)^2} \int |F_{k_0 k}|^2 \delta(\omega - \omega_k) d^3k \quad (31)$$

where  $\omega$  is the frequency of the mode  $k_0$  and  $F_{k_0 k}$  is the Fourier transform of the scattering potential  $V$ . In the presence of a strong perturbation the plane wave magnon states  $|k\rangle$  are replaced by the wavefunction

$$|\psi_k\rangle = |k\rangle + G^0 V |\psi_k\rangle \quad (32)$$

The linewidth can be conveniently calculated by introducing the  $t$ -matrix as the operator which acts on the unperturbed states  $|k\rangle$  to give the same result as  $V$  acting on the distorted state  $|\psi_k\rangle$

$$T |k\rangle = V |\psi_k\rangle \quad (33)$$

so that  $T$  accounts for multiple impurity scattering to all orders. From From eq. (32) and (33) we have

$$T = (1 - VG^0)^{-1} V \quad (34)$$

Then multiple scattering results are included by replacing  $V$  by  $T$  in the first order time dependent perturbation expression for the transition probability; i.e., the squared matrix element becomes

$$|\langle k | T | k_0 \rangle|^2 = \langle \psi_k | V | k_0 \rangle|^2 \quad (35)$$

Of course, far from a scattering resonance or a bound state  $T \approx V$  and the modification to ordinary first order perturbation theory is small. However, here the effect is enormous, as the existence of a local mode implies, and as a consequence the linewidth is enhanced by three orders of magnitude<sup>34</sup>. The frequency dependence of the observed linewidth is



accounted for by the increasing density of degenerate magnon states with increasing frequency. Fig. 11 shows the calculated linewidth for

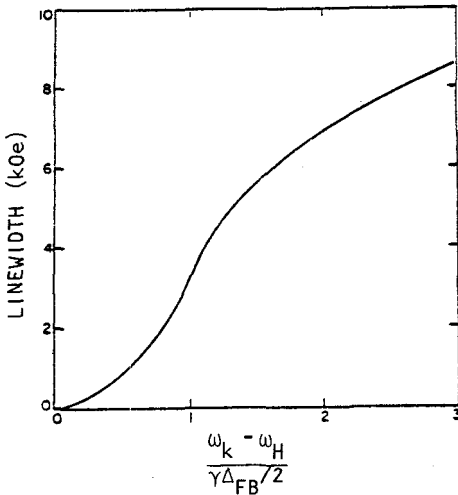


Fig.11 - Linewidth due to two-magnon impurity multiple scattering in 0.5% Mn:FeF<sub>2</sub> as a function of position of the magnetic mode relative to the bottom of the spin wave band<sup>34</sup>.

$x = 0.5\%$  as a function of the mode frequency relative to the bottom of the magnon band, in units of  $\Delta_{FB}/2$  (the width of the spinwave manifold). We note that the contributions from exchange, anisotropy and g-factor scattering are equally important for the linewidth, which has the magnitude of a few kOe and is strongly frequency dependent. In Fig.12 the experimentally measured transmission host mode lineshape obtained for a sample with  $x = 0.5$  at.% is compared to theoretical predictions of the polariton model with a frequency dependent relaxation parameter given by the above theory. As can be seen, the agreement between theory and experiment is remarkably good.

## 8. CONCLUDING REMARKS

We have seen in this review how rich can be the physics of the dynamics of spin excitations in a simple magnetic system with a substitutional impurity, by way of the particularly interesting and well-studied example, FeF<sub>2</sub>:Mn. The variety of phenomena studied and information available is remarkable. We have indicated that a single, relatively simple, Hamiltonian (10) is quantitatively compatible with all

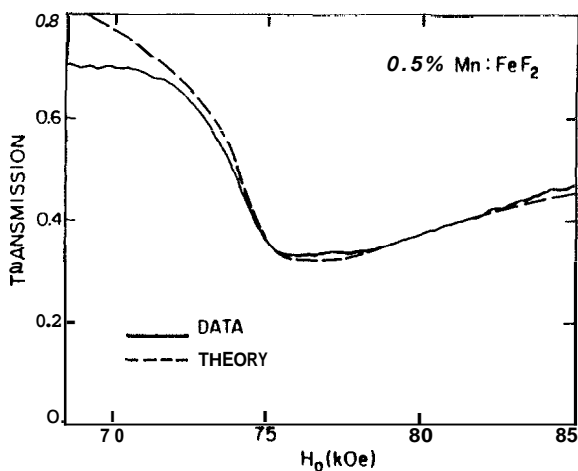


Fig.12 - Comparison of transmission data from a 80  $\mu\text{m}$  thick sample of 0.5 at.% Mn:FeF<sub>2</sub> (solid curve) with the theoretical prediction of a polariton model with a frequency dependent relaxation parameter obtained from the two-magnon impurity multiple scattering calculation<sup>34</sup>.

available observations. This and closely related systems can continue to be used as quantitatively understood models of magnetic insulators.

The authors acknowledge all of our collaborators named explicitly in the reference list below. We are specially grateful to Professor V. Jaccarino for many illuminating suggestions and discussions. This work was supported by CNPq, FINEP, CAPES and NSF through grant no DMR-80-17582.

#### REFERENCES

1. An early review of this area is in the book *Localized Excitations in Solids*, edited by F.R. Wallis, (Plenum, New York, 1968).
2. T. Wolfram and F. Callaway, Phys. Rev. 130, 2207 (1963).
3. J.M. Lifshitz, J. Exp. Theor. Phys. (JETP) 17, 1017 (1947); *Ibid.*, 17, 1076 (1947); *Ibid.*, 18, 293 (1948).
4. G.F. Koster and J.C. Slater, Phys. Rev. 96, 1208 (1954).
5. P.G. Dawber and R.J. Elliot, Proc. Phys. Soc. 273, 222 (1963).
6. W.J.L. Buyers, R.A. Cowley, T.M. Holden, and R.W.H. Stevenson, J. Appl. Phys. 39, 1118 (1968); E.C. Svensson, T.M. Holden, W. J. L. Buyers, R.A. Cowley and R.W.H. Stevenson, Solid State Commun. 7, 1693 (1969).
7. P.Moch. G. Parisot, R.E. Dietz, and H.J. Guggenheim, Phys.Rev.Lett. 21, 1596 (1968); A.Oseroff and P.S. Pershan, Phys. Rev. Lett. 21,

- 1593 (1968); also in *Light Scattering in Solids*, edited by M. Balkanski (Flammarion, Paris, 1971).
8. R. Weber, Phys. Rev. Lett. 21, 1260 (1968).
  9. M. Butler, V. Jaccarino, N. Kaplan, and H.J. Guggenheim, Phys. Rev. B 1, 3058 (1970).
  10. R.A. Cowley and W.J.L. Buyers, Rev. Mod. Phys. 44, 406 (1972).
  11. W.J.L. Buyers, T.M. Holden, E.C. Svensson, R.A. Cowley, and R.W.H. Stevenson, Phys. Rev. Lett. 27, 1442 (1971); E.C. Svensson, W.J.L. Buyers, T.M. Holden, R.A. Cowley, and R.W.H. Stevenson, in *Magnetism and Magnetic Materials - 1971* (Chicago), Proceedings of the 17th Annual Conference on *Magnetism and Magnetic Materials*, edited by D. C. Graham and J.J. Rhyne (American Institute of Physics, New York, 1972), p.1315; R.A. Cowley, in *Magnetism and Magnetic Materials - 1975* (Philadelphia), Proceedings of the 21st Annual Conference on *Magnetism and Magnetic Materials*, edited by J.J. Becker, G.H. Lander, and J.J. Rhyne (AIP, New York, 1976), p. 243.
  12. J.P. Gosso and P. Moch, in *Proceedings of the 3rd International Conference on Light Scattering in Solids*, Campinas, 1975, edited by M. Balkanski, R.C.C. Leite and S.P.S. Porto (Flammarion, Paris, 1976).
  13. R.W. Sanders, V. Jaccarino, and S.M. Rezende, Solid State Commun. 28, 907 (1978); R.W. Sanders, R.M. Belanger, M. Motokawa, V. Jaccarino, and S.M. Rezende, Phys. Rev. B 23, 1190 (1981).
  14. S.M. Rezende, C.B. de Araujo, and E. Montarroyos, Solid State Commun. 35, 627 (1980).
  15. S.M. Rezende and E.F. da Silva, Jr., Phys. Rev. B (to be published).
  16. R.M. White and C.M. Hogan, Phys. Rev. 167, 480 (1968).
  17. B. Koiller and S.M. Rezende, Phys. Rev. B 22, 3325 (1980).
  18. S.M. Rezende, Phys. Rev. B 27, 3032 (1983).
  19. S.V. Tyablikov, *Methods in the Quantum Theory of Magnetism* (Plenum, New York, 1967).
  20. D.N. Zubarev, Usp. Fiz. Nauk, 71, 71 (1960) [*Sov. Phys.-Usp.*, 3, 320 (1960)].
  21. S.W. Lovesey, J. Phys. C 1, 102 (1968).
  22. T. Tonegawa, Prog. Theor. Phys. 40, 1195 (1968).
  23. E. Shiles and D. Hone, J. Phys. Soc. Jpn. 28, 51 (1970).
  24. A.S. Prokhorov and E.G. Rudashevskii, Zh. Eksp. Teor. Fiz. Pis'ma

- Red. 22, 214 (1975) [JETP lett. 22, 99 (1975)]; M. A. Ivanov, Y.G. Pogorelov, V.M. Loktev, K.N. Kocharyan, A. S. Prokhorov, and E.G. Rudashevski, Solid State Commun. 33, 623 (1980).
25. V.V. Eremenko, V.M. Naumenko, S.V. Petrov and V.V.Pishko, Zh. Eksp. Teor. Fiz. 82, 813 (1982) [JETP 55, 481 (1982)].
  26. U. Dürer and B. Uwira, J. Phys. C12, L 793 (1979).
  27. R.W. Sanders, D.Paquette, V.Jaccarino and S.M. Rezende, Phys. Rev. B 10, 132 (1974).
  28. C. Wiecko and D.Hone, J. Phys. C13, 3883 (1980).
  29. S.M. Rezende, D. Hone, and R.M. Toussaint, Phys. Rev. B 29, 1638 (1984).
  30. P. Thayamballi and D.Hone, Phys. Rev. B 27, 2924 (1983).
  31. S.W. Lovesey, J. Phys. C 5, 2769 (1972).
  32. M. Motokawa, C. Uyeda, A. Otsuka, M. Date, and R.M. Toussaint, to be published.
  33. R.M.Belanger, D. Hone and M. Motokawa, Phys. Rev. B 25, 3186 (1982).
  34. R.M.Toussaint, D. Hone, V. Jaccarino, and S.M. Rezende, Phys. Rev. B 30, 3859 (1984).
  35. R. Loudon and P. Pincus, Phys. Rev. 132, 673 (1963).

#### Resumo

Alguns isolantes magnéticos com impurezas têm modo local com energia logo-abaixo da banda de onda de spin. Experiências recentes de alta resolução no infravermelho distante e de espalhamento Raman em  $\text{FeF}_2:\text{Mn}^{2+}$  revelaram vários novos efeitos interessantes não observados no caso mais comum em que o modo da impureza está longe da banda. Entre esses efeitos estão um grande aumento da resposta da impureza, rápida relaxação do modo local e forte dependência com a frequência do modo de AFMR. Todos esses efeitos podem ser explicados quantitativamente com uma teoria de funções de Green para a dinâmica do modo local. Neste trabalho apresentamos uma revisão da grande variedade de observações experimentais nesse sistema e da teoria que os explica.